RevMexAA (Serie de Conferencias), **29**, 104–106 (2007)

VLT/SINFONI SPECTROSCOPY OF THE SUPERANTENNAE

J. Reunanen,[1] V. D. Ivanov,[2] L. E. Tacconi-Garman,[3] and L. J. Tacconi[4]

RESUMEN

Presentamos los resultados de espectroscopía de campo integral en bandas H y K VLT/SINFONI de IRAS 19254-7245 (Superantennae), una ULRIG cercana con un AGN embebido. Los mapas de las líneas, campos de velocidades y mapas de dispersión de velocidades se presentan para varias líneas de emisión. Las proporciones de las líneas de emisión de H2 son consistentes con la excitación térmica, debida probablemente a choques.

ABSTRACT

We present the results of H- and K-band VLT/SINFONI integral field spectroscopy of IRAS 19254-7245 (Superantennae), a nearby ULIRG with an embedded AGN. The line maps, velocity fields and velocity dispersion maps are presented for several emission lines. H_2 emission line ratios are consistent with thermal excitation, probably due to shocks.

Key Words: **GALAXIES: SEYFERT — GALAXIES: STARBURST**

1. INTRODUCTION

The superantennae (IRAS 19254-7245, $z \simeq 0.062$) is an interacting galaxy pair where the two components are separated by ∼2 kpc. The system is best known for the antennae, which are far longer - ∼350 kpc - than in Antennae galaxy. While the northern nucleus is in post-starburst phase, the southern nucleus is much brighter in IR and is powered by starburst with an embedded AGN. As in many other ULIRGs, it's not clear whether the the galaxy is AGN- or starburst-dominated (Genzel et al. 1998; Charmandaris et al. 2002).

2. OBSERVATIONS AND DATA REDUCTION

The Superantenna was observed with the near-IR integral field spectrograph SINFONI on VLT (Paranal, Chile) in August 2004. The total integration time was 14000 s in K ($R \simeq 4500$) and 1800 s in H ($R \simeq 2000$). The average V-band seeing during the observations was 0.″94 in K band and 0.″77 in H band. At the time of the observations, a 2048^2 pixel engineering grade camera was used with 250 mas/pixel observations allowing a field of view of $8{\times}8''$.

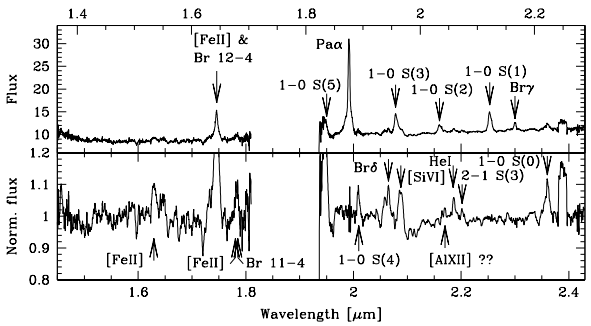

Fig. 1. The nuclear HK spectrum of Superantennae (*top*) and the residual spectrum after normalization and subtracting the most luminous emission lines (Paα, Brγ, H_2; *bottom*).

The data reduction was done with *spred* software developed by MPE. The data was sky subtracted, bad pixel corrected and divided by flatfield. The geometric distortions were corrected based on North-South test frames. The wavelength calibration was based on both arc lamp calibration frames and OH night sky lines. The residal sky background was removed by calculating a median value along the edges of the cubes at each spectral plane and subtracting this. Finally, the flux calibration was done by comparison with broad-band images (Vanzi et al. 2002) and telluric standards.

3. DISCUSSION

The 1.5 - 2.4 μm spectrum of the nucleus of Superantenna is shown in Figure 1. The emission lines detected arise mostly from ionized gas ([FeII], Paα,

[1]Leiden Observatory, Leiden University, PO Box 9513, 2300 RA Leiden, The Netherlands (reunanen@strw.leidenuniv.nl).
[2]European Southern Observatory, Alonso de Cordova 3107, Santiago 19, Chile.
[3]European Southern Observatory, Karl Schwarzschild-strasse 2, 85748 Garching, Germany.
[4]Max-Planck-Institut für extraterrestrische Physik, Postfach 1312, 85741 Garching, Germany.

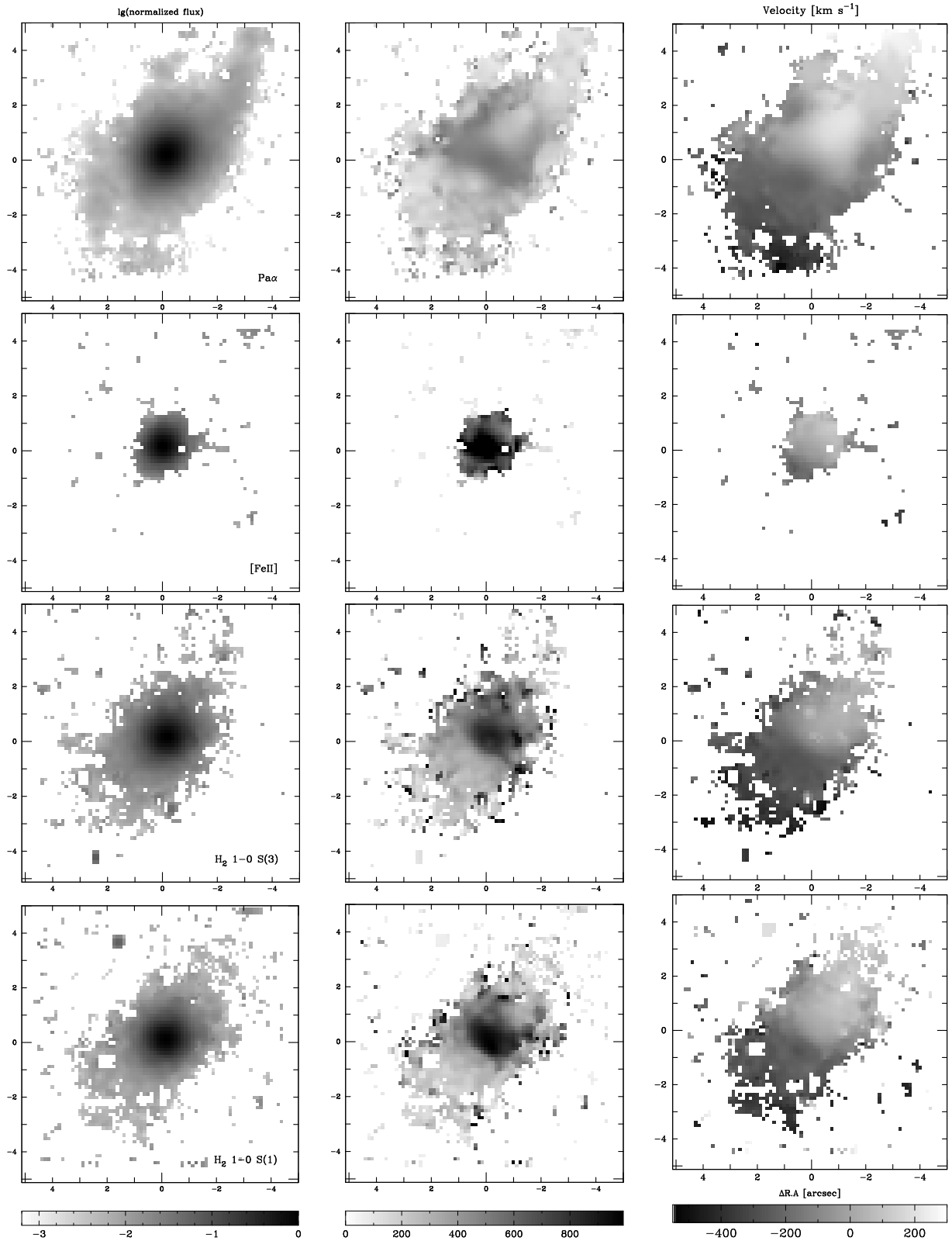

Fig. 2. The logarithmic flux normalized to the nucleus (*left*), the gaussian FWHM of the line (*middle*) and the velocity relative to the systemic velocity (*right*), for Paα (*top*), FeII, H_2 1-0 S(3) and H_2 1-0 S(1) (*bottom*).

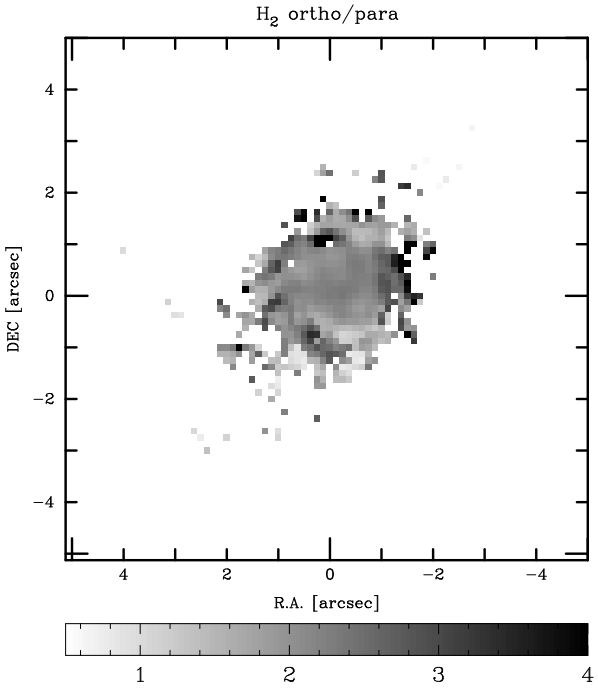

Fig. 3. H_2 ortho/para ratio map for Superantenna.

Brγ, Brδ, HeI) or molecular material (H_2 1-2 and 2-1 transitions). In addition, carefull study reveals the presence of high-excitation coronal lines [SiVI] and [AlIX] (detected at 12σ level).

The strongest emission line by far is Paα, which is badly fitted with a single gaussian. Similarily, multiple components (three or more; Vanzi et al. 2002; Colina, Lipari & Macchetto 1991) have been used to approximate optical emission lines. While a two-component fit to Paα produces acceptable results in the sense that the residuals (red asymmetry) can be readily explained by obscured broad line region, the similarity with the Hα suggests this is not the case. However, we note that the FWHM of the broader component in the two-component fit is similar to possible detection of polarized broad Hα by Pernechele et al. (2003).

The emission line fluxes, gaussian FWHMs and velocity fields for Paα 1.87 μm, [FeII] 1.64 μm and the H_2 lines (1-0 S(1) 2.12 μm and 1-0 S(3) 1.95 μm) are shown is Figure 2. The most extended emission line, Paα, shows spiral structures in South-East and North-West coinciding with the dusty spirals visible in *HST* archive images. The spirals are composed of several star forming knots, some of which are also detected in H_2. A separate star forming knot is detected in North. The star forming rate estimated from Paα is 50 $M_\odot$ yr^{-1}.

Only 1-0 and 2-1 H_2 transitions can be detected, and the line ratios are consistent with thermal excitation. This is contrary to Davies et al. (2003), who detected even 3-2 transitions in a sample of ULIRGs and derived very high excitation temperatures based on 2-1 and 3-2 transitions, indicating UV fluorescence in dense clouds. Thermal excitation probably due to shocks is also supported by low Brγ/1–0 S(1) ratio. The average column density of molecular hydrogen within the 5×5 pixel region is $\sim 10^{23}$ m^{-2}, corresponding to the total mass of hot excited molecular hydrogen of 10^4 $M_\odot$, which is many magnitudes below the mass of the available molecular material (3×10^{10} $M_\odot$; Mirabel et al. 1990)

The H_2 ortho/para ratio map (calculated from 1-0 S(1), S(2) and S(3) lines) is shown in Figure 3. The ratio is higher closer to the nucleus than further out, indicative of higher gas densities surrounding the nucles. The spiral like pattern present in ortho-para map can also be detected in emission line ratio maps.

REFERENCES

Charmandaris, V., et al. 2002, A&A, 391, 429
Colina, L., Lipari, S., & Macchetto, F. 1991, ApJ, 379, 113
Davies, R. I., Sternberg, A., Lehnert, M., & Tacconi-Garman, L. E. 2003, ApJ, 597, 907
Genzel, R., et al. 1998, ApJ, 498, 579
Mirabel, I. F., Booth, R. S., Johansson, L. E. B., Garay, G., & Sanders, D. B. 1990, A&A, 236, 327
Pernechele, C., et al. 2003, MNRAS, 338, L13
Vanzi, L., Bagnulo, S., Le Floc'h, E., Maiolino, R., Pompei E., & Walsh W. 2002, A&A, 386, 464